Bis(diphenylamino)-9,9′-spirobifluorene functionalized Ir(III) complex: a conceptual design *en route* to a three-in-one system possessing emitting core and electron and hole transport peripherals†

Hsiao-Fan Chen,[a] Ken-Tsung Wong,*[a] Yi-Hung Liu,[a] Yu Wang,[a] Yi-Ming Cheng,[b] Min-Wen Chung,[b] Pi-Tai Chou*[b] and Hai-Ching Su[c]

Received 3rd July 2010, Accepted 27th September 2010
DOI: 10.1039/c0jm02097d

Conceptual design of a three-in-one (luminescence chromophore with electron and hole transports) system was demonstrated by a functionalized Ir(III) complex **3**, in which 4,5-diazafluorene and bis(diphenylamino) serve as electron and hole transporting sites, respectively. The poor emission quantum yield of **3** was systematically examined *via* a series of photophysical studies in combination with theoretical approaches. The far lifting of the π-electron from -NPh_2 renders virtually no ^{3}MLCT contribution to the lowest transition in the triplet manifold as compared with that of the parent model **2** without amino substituents. With an empirical approach, we conclude that an energy gap law may account for the major deactivation process. A light-emitting electrochemical cell (LEC) device based on **3** shows peak EQE, peak current efficiency and peak power efficiency at 2.4 V of 0.020%, 0.013 cd A^{-1} and 0.017 lm/W, respectively. The low device efficiencies are in accordance with the low PL quantum yield, stemming from the ligand-centered radiationless deactivation. The conceptual design presented here should provide valuable information for future progress *en route* to an ideal three-in-one system suited for OLEDs.

Introduction

Transition-metal complexes showing strong phosphorescent emission at RT have recently received much attention due to their intriguing photophysical properties[1] and perspectives for fabricating organic light emitting diodes (OLEDs) suited for full colour displays, white-emitting devices for general lighting applications and backlight panels of future liquid crystal displays.[2] The emerging demand for high efficiency phosphors has inspired the investigation of late transition metal complexes such as Ir(III), Os(II) and Pt(II), *etc.* incorporated with a variety of chelating chromophores.[3] Imposed by the central heavy metal atom, the enhanced spin–orbit coupling would effectively promote singlet-to-triplet intersystem crossing as well as subsequent radiative decay, yielding room temperature phosphorescence. The resulting phosphorescent OLEDs in theory would give unitary efficiency in the upper limit, which is far greater than the 25% theoretical limit predicted for those using fluorescent emitting materials.[4]

For OLED applications, the intrinsic triplet–triplet annihilation process makes these phosphorescent materials particularly suited as dopants. Thus, in yet another parallel approach, development of the host materials for electron and/or hole transport is equally important. In this regard, our recent studies have demonstrated the excellence of luminescence (fluorescence) and electron/hole transport properties for spirobifluorenes.[5] The synthetic versatility makes feasible the design of chelating

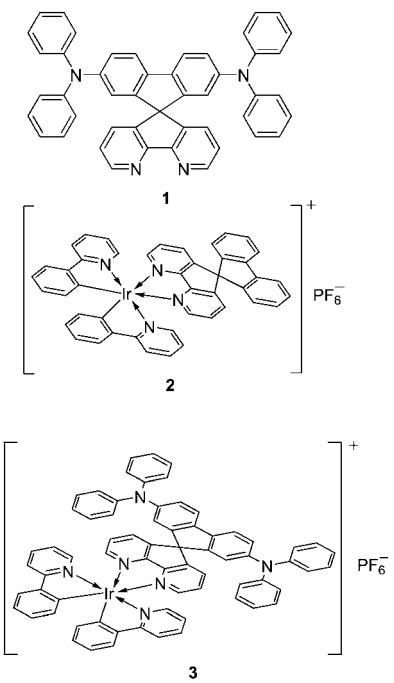

Scheme 1

[a]*Department of Chemistry, National Taiwan University, Taipei, 106, Taiwan. E-mail: kenwong@ntu.edu.tw; Fax: +886 2 33661667; Tel: +886 2 33661665*
[b]*Department of Chemistry, National Taiwan University, Taipei, 106, Taiwan. E-mail: chop@ntu.edu.tw; Fax: +886 2 23695208*
[c]*Institute of Lighting and Energy Photonics, National Chiao Tung University, Tainan, 71150, Taiwan*

† Electronic supplementary information (ESI) available: ^{1}H and ^{13}C NMR spectra of complex **3** and expanded UV-Vis absorption spectra of complex **2** and **3**. CCDC reference numbers 783216. For ESI and crystallographic data in CIF or other electronic format see DOI: 10.1039/c0jm02097d

spirobifluorenes suitable for incorporation into transition metal complexes. As such, it is of great interest to design a unique three-in-one system capable of acting as an electron and hole transporting material as well as exhibiting active phosphorescence emission. A three-in-one system may possess advantages over a physically blended one. Direct mixing of functional materials may cause inevitable issues such as phase separation, which can result in poor film quality, and uncontrollable molecular packing in the solid state, impeding the carrier-transport behavior. Herein, we report a conceptual design and synthesis of a bis(diphenylamino)-9,9′-spirobifluorene functionalized Ir(III) complex, complex **3** (Scheme 1), in which the 4,5-diazafluorene and diphenylamino substituents act as electron and hole transporting materials, respectively, while the whole Ir(III) complex serves as a luminescence unit. Structural characterization, thermodynamics and photophysical properties have been carried out in a comprehensive manner. These, in combination with the computational approaches, provide valuable information for future design toward an ideal three-in-one system for OLED applications.

Experimental

Synthesis

Compounds **1**[6] and **2**[7] were prepared following literature procedures.

Synthesis of complex **3** (Scheme 2): A mixture of bis-(μ)-chlorotetrakis(2-phenylpyridinato-C^2,N)diiridium(III) (1.0 mmol, 0.7 g) and 4,5-diaza-2′,7′-bis(diphenylamino)-9,9′-spirobifluorene (2.2 mmol, 0.7 g) was dissolved in 1,2-ethanediol (20 mL) under argon and stirred for 16 h at 150 °C. The reaction mixture was cooled to room temperature and an aqueous solution of NH_4PF_6 (10 g in 100 mL deionised water) was added to yield a red suspension. The solid was then filtered off and dried in an oven (80 °C) for 12 h. The crude product was purified by column chromatography on silica gel (CH_2Cl_2–MeCN = 10/1) to give compound **3** (1.24 g, 76%) as an orange solid. ^{1}H NMR (DMSO-d_6, 400 MHz) δ 8.21 (d, J = 8.0 Hz, 2H), 7.89∼7.85 (m, 6H), 7.77 (d, J = 8.0 Hz, 2H), 7.57–7.52 (m, 6H), 7.18 (t, J = 7.6 Hz, 8H), 7.00–6.96 (m, 8H), 6.89–6.85 (m, 10H), 6.61 (t, J = 6.6 Hz, 2H), 6.36 (d, J = 1.6 Hz, 2H), 6.23 (d, J = 7.2 Hz, 2H);^{13}C NMR (DMSO-d_6, 100 MHz) δ 167.1, 161.4, 149.1, 148.8, 147.3, 147.1, 145.0, 144.6, 143.5, 143.1, 139.3, 136.3, 135.1, 131.9, 130.3, 129.8, 129.2, 125.2, 124.5, 124.2, 124.0. 123.8, 122.9, 122.0, 120.2, 118.3, 66.4; MS (*m*/*z*, FAB$^+$) 1153 (40), 501 (50), 154 (100); HRMS (*m*/*z*, FAB$^+$) Calcd for $C_{69}H_{48}N_6PIr$ 1153.3570 [M$^+$], found 1153.3573. **3** was further confirmed by single crystal crystallographic analysis, details of which are described below.

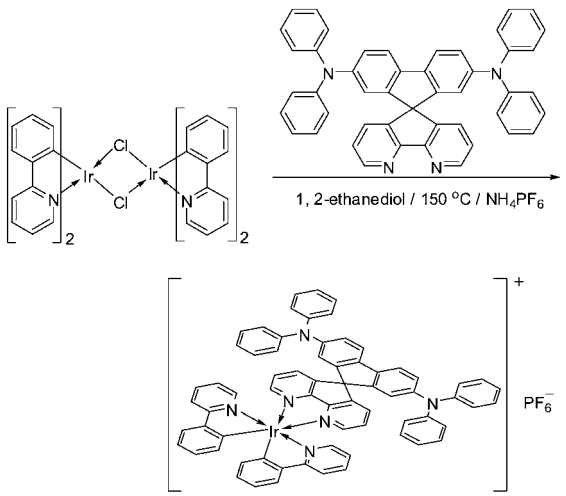

Scheme 2 Synthetic pathways and structures of complex **3**.

Measurements

^{1}H and ^{13}C NMR spectra of compounds were collected on a 400 MHz spectrometer at room temperature. CVs were performed at a scan rate of 100 mV s^{-1} using a glassy carbon working electrode and Ag/AgCl as a reference electrode. Oxidation CV was performed in CH_2Cl_2 with 0.1 M of nBu$_4$NPF$_6$ as a supporting electrolyte. For reduction CV, 0.1 M of nBu$_4$ClO$_4$ in THF was used as a supporting electrolyte.

Steady-state absorption and emission spectra were recorded with a Hitachi (U-3310) spectrophotometer and an Edinburgh (FS920) fluorimeter, respectively. Nanosecond to microsecond lifetime studies were performed with a photon-counting system with a hydrogen-filled or nitrogen lamp as the excitation source. The emission decays were analyzed by the sum of exponential functions, which allows partial removal of the instrument time broadening and consequently provides a temporal resolution of ∼200 ps.

Crystal structure determination

Crystallographic data were collected at 295(2) K on a NONIUS Kappa CCD diffractometer using graphite-monochromatized Mo-Kα radiation (λ = 0.71073 Å). Cell parameters were retrieved and refined using HKL Denzo & Scalepack software on all observed reflections.[8] Data reduction was performed with the HKL Denzo & Scalepack software. The structures were solved and refined with SHELX programs.[9] The hydrogen atoms were included in calculated positions and refined using a riding mode.

Computational methodology

Geometry optimizations of studied complexes were carried out using the density functional theory (DFT) with the B3LYP hybrid functional.[10] A "double-ζ" quality basis set consisting of Hay and Wadt's effective core potentials (LANL2DZ)[11] was employed for the Ir atom, and a 6-31G* basis set,[12] for H, C, and N atoms. The relativistic effective core potential (ECP) replaced the inner core electrons of the Ir(III) metal atom, leaving the outer core ($5s^25p^6$) electrons and the $5d^6$ valence electrons to be concerned. Time-dependent DFT (TDDFT) calculations using the B3LYP functional were then performed based on the optimized structures at ground states to probe the emissive properties.[13] All calculations were carried out using Gaussian 03[14] associated with the AOMix program[15] to estimate the compositions of molecular orbitals in terms of the constituent chemical fragments involved in the electronic transition.

Fabrication and characterization of LEC devices

Neat films of **3** were spin-coated onto quartz substrates from the acetonitrile solutions. The thickness of spin-coated films was ~100 nm, as measured by ellipsometry. PL spectra of thin films were measured with a fluorescence spectrophotometer (HITACHI F9500). ITO-coated glass substrates were cleaned and treated with UV/ozone prior to coating of the emissive layer. The preparation of solutions of **3** and spin-coating of thin films (~100 nm) of **3** were performed in the nitrogen atmosphere of a glove box. To reduce the turn-on time of the LEC device, 19 wt.% ionic liquid [$BMIM^+(PF_6^-)$] was added to enhance the ionic conductivity of thin films.[16] After spin coating, the thin films were then baked at 70 °C for 15 h, followed by thermal evaporation of a 150 nm Ag top contact in a vacuum chamber (~10^{-6} Torr). The electrical and emission characteristics of LEC devices were measured using a source-measurement unit and a Si photodiode calibrated with a Photo Research PR-650 spectroradiometer. Measurements of time-dependent electroluminescence (EL) characteristics of devices were performed under a constant bias voltage (2.4 V). The EL spectra were taken with a calibrated CCD spectrograph.

Results and discussion

Crystals of complex **3** suitable for X-ray diffraction analysis were obtained by the double-layer method using dichloromethane and diethyl ether. Complex **3** was crystallized in the monoclinic crystal structure with a space group of *C*2/*c* (Table 1). As depicted in Fig. 1, complex **3** with two cyclometalated 2-phenylpyridine (*C*^*N*) ligands and one 4,5-diaza-2′,7′-bis(diphenylamino)-9,9′-spirobifluorene (*N*^*N*) ligand exhibits a distorted octahedral geometry around the Ir center as indicated by the small bite angles of C(11)-Ir(1)-N(1) [81.0(6)°], C(11A)-Ir(1)-N(1A) [81.0(6)°], N(2)-Ir(1)-N(2A) [80.4(6)°], and twisted bond angles of N(1)-Ir(1)-N(1A) [170. 6(6)°], C(11)-Ir(1)-N(2A) [174.2(5)°], C(11A)-Ir(1)-N(2) [174.2(5)°]. The Ir–N bond distances between the Ir center and 4,5-diaza-2′,7′-bis(diphenylamino)-9,9′-spirobifluorene, Ir(1)-N(2) [2.203(14) Å] and Ir(1)-N(2A) [2.203(14) Å], are significantly longer than those between the Ir center and 2-phenylpyridine, Ir(1)-N(1) [2.047(9) Å] and Ir(1)-N(1A) [2.047(9) Å]. This can be attributed to the anionic nature of the cyclometalated 2-phenylpyridine ligands, which have stronger interaction with the cationic Ir(III) ion. Fig. 2 illustrates the crystal packing structure in a unit cell of complex **3** seen along the *b*-axis. The long Ir–Ir distances of 13.29 Å along the *b*-axis and 13.98 Å along the *c*-axis, respectively, indicate the lack of significant intermolecular interactions, the result of which can be ascribed to the bulkiness of 4,5-diaza-2′,7′-bis(diphenylamino)-9,9′-spirobifluorene ligand. The calculated distance between N(3) (or N(3A)) and Ir(1) is 8.15 Å, which is suitable for efficient electron transfer process.

Table 1 The crystal data of complex **3**

	3
Empirical formula	$C_{69}H_{48}F_6IrN_6P$
Formula weight	1298.30
Crystal dimensions/mm^3	0.15 × 0.10 × 0.10
Crystal system	Monoclinic
Space group	*C*2/*c*
a/Å	24.575(3)
b/Å	13.3527(12)
c/Å	20.4212(18)
α (°)	90
β (°)	105.367(7)
γ (°)	90
Cell volume/Å^3	6461.5(11)
Z	4
Density (calc)/g cm^{-3}	1.335
F(000)	2600
Temperature/K	295(2)
Wavelength/Å	0.71073
No. of refln collected	14683
No. of indep refln (R_{int})	5674(0.1203)
$R(F)$, $wR2$ [$I > 2\sigma(I)$]	0.1058, 0.2521
$R(F)$, wR_2 (all data)	0.1947, 0.3105

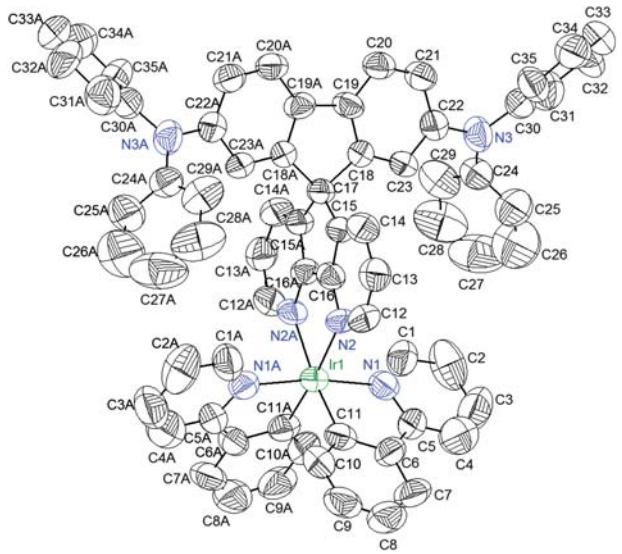

Fig. 1 The molecular structure of complex **3**. Thermal ellipsoids are drawn at 50% probability.

Prior to photophysical measurements, the electrochemical characteristics of compound **1–3** were probed by cyclic voltammetry (CV) and the results are summarized in Table 2. Two reversible oxidation potentials were detected for compound **1** (0.20 and 0.49 V) and compound **3** (0.31 and 0.47 V), which could be assigned to the oxidation of triarylamine moieties. The

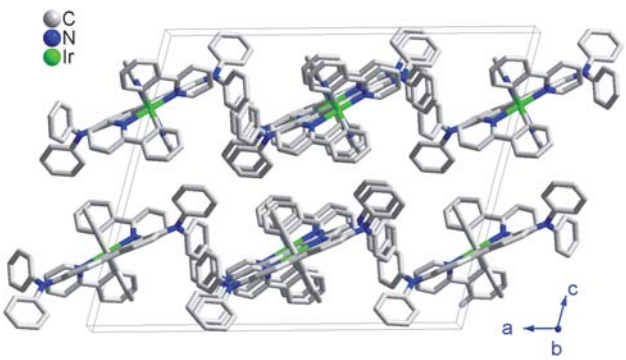

Fig. 2 Crystal packing of complex **3** in a unit cell. The solvent molecules, counter anions (PF_6^-), and hydrogen atoms are omitted for clarity.

Table 2 Cyclic voltammetry results

	1	2	3
$E_{1/2}^{ox}$ (V)[a]	0.20, 0.49 V[d]	0.88 V[f]	0.31, 0.47, 0.87 V[f]
$E_{1/2}^{red}$ (V)[b]	−2.61 V[e]	−1.76 V[g]	−1.75 V[g]
$\Delta E_{1/2}$ (V)[c]	2.81 V	2.64 eV	2.06 eV

[a] Oxidation potential *vs.* ferrocene/ferrocenium redox couple. [b] Reduction potential *vs.* ferrocene/ferrocenium redox couple. [c] The electrochemical gap $\Delta E_{1/2}$ is the difference between $E_{1/2}^{ox}$ and $E_{1/2}^{red}$ corrected by potentials of the ferrocene/ferrocenium redox couple. [d] 0.1 M $TBAPF_6$ in CH_2Cl_2. [e] 0.1 M TBAP in THF. [f] 0.1 M $TBAPF_6$ in acetonitrile. [g] 0.1 M TBAP in acetonitrile.

pronounced potential differences between the first and second oxidation of **1** and **3** indicate that efficient resonance delocalization of the radical cation occurs in the diphenylamino group-containing branch. The slightly higher first oxidation peak of **3** as compared to that of **1** can be possibly attributed to the electron-withdrawing effect *via* the coordination of diazafluorene to an Ir center. The oxidation potentials of the iridium centers of compounds **2** and **3** are observed to be 0.88 V and 0.87 V, respectively. According to previous studies,[6,7] the LUMO of compound **1** is mainly located on the diazafluorene moiety, in which the energy level will be significantly perturbed by metal coordination. Indeed, the reductions of **2** and **3** exhibit evident lower potential at *ca.* −1.75 V as compared to that of compound **1** (at −2.61 V).

Fig. 3 shows the absorption and emission spectra of molecules **1–3** in acetonitrile. As for the absorption spectra of **1** and **3**, the shorter wavelength region (350–380 nm) for both molecules with large absorptivity of $\sim 10^4$ M^{-1} cm^{-1} is reasonably ascribed to the corresponding diphenylamino-capped fluorene $\pi\pi^1$* transition, which is obscure in complex **2** due to the lack of diphenylamino substituent. Both complexes **2** and **3** exhibit similar absorption features in the lower lying absorption bands of >400 nm that is apparently missing in the free ligands (*cf.* **1**). As supported by their extinction coefficients in the range of $\sim 10^3$ M^{-1} cm^{-1}, we then tentatively assigned these bands to the metal-to-ligand charge transfer (MLCT) mixed perhaps with certain $\pi\pi$* (intra-

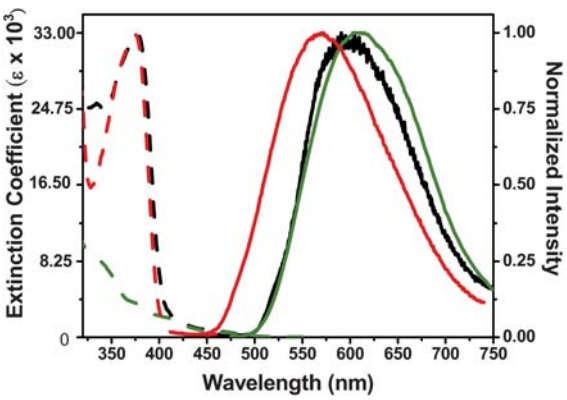

Fig. 3 UV-Vis absorption (dashed lines) and emission (solid lines) spectra of complexes **1** (red), **2** (green) and absorption of **3** (black) in acetonitrile. Note that the spectra were acquired under degassed conditions and the intensity has been normalized. The emission of **3** was measured in 77 K glassy ethanol.

ligand or ligand-to-ligand charge transfer) transition character (*vide infra*).

In comparison to **3**, an additional absorption tail (>500 nm) with an extinction coefficient (ε) of ≤100 M^{-1} cm^{-1} for **2** (see ESI†) suggests it originates from a triplet manifold. The result indicates a greatly enhanced S_0–T_n (n ∼ 1, *vide infra*) transition in **2** due to an enhanced spin–orbit coupling, *i.e.* greater MLCT contribution, and hence it becomes a partially allowed transition. Knowing that -NPh_2 is a strong electron donating group, the results simply imply a greater π electron contribution to the HOMO for **3**, manifesting the salient differences between **2** and **3** in the lower lying electronic transitions. Further support of this viewpoint is given by the following luminescent studies and theoretical approaches.

In degassed CH_3CN solution, highly emissive room-temperature phosphorescence with a peak wavelength at 610 nm was observed for complex **2**. The quantum yield and lifetime were measured to be ∼40% and ∼0.49 ± 0.05 μs, respectively. Conversely, to the best of our attempts, the emission of **3** unfortunately could not be resolved. We thus made a further attempt to acquire the corresponding luminescence at cryogenic temperature. Upon lowering the temperature to 77 K, a weak phosphorescence was resolved at 595 nm in the frozen, glassy ethanol matrix. The emission yield and lifetime for **3** were measured to be $\sim 1.0 \times 10^{-3}$ and 2.3 μs, respectively. By knowing the emission yield $\Phi_p = \tau_{obs}/\tau_r$, the radiative lifetimes of **2** and **3** were deduced to be 1.2 μs and 2.3 ms, respectively.

The more than three order of magnitude increase (*cf.* **2**) in the radiative lifetime in **3** again supports the early proposal of its dominant $\pi\pi$* character for the $T_1 \rightarrow S_0$ transition. The exceedingly long radiative lifetime (2.3 ms) in **3** is thus subject to any radiationless deactivation pathways, among which one possible efficient quenching process may be ascribed to the increase of the rotational degrees of freedom with *e.g.* the additional NPh_2 functional group. Nevertheless, **3** still exhibits weak emission intensity in solid state (<1%) as well as in 77 K ethanol solid matrix ($\Phi_p \sim 1.0 \times 10^{-3}$, *vide supra*), indicating that there exist certain radiationless deactivation channels other than quenching by the large amplitude motions (*vide infra*).

Further insights into the photophysical properties of the studied complexes are gained from a theoretical approach (B3LYP/6-31G* associated with LANL2DZ effective core potentials, see experimental section). The features of the frontier HOMO and LUMO orbitals mainly involved in the lower lying electronic transitions are depicted in Fig. 4. As shown in Fig. 4, the HOMO → LUMO transition for **2** was contributed to a large extent by the MLCT (metal d_π to the bipyridine moiety, ∼35.4%) mixed with the $\pi\pi$* (LLCT) transition mainly from the 2-phenylpyridine to the bipyridine moiety. In sharp contrast, however, the results shown in Fig. 4 clearly indicate that the lowest lying transitions for **3** in both singlet and triplet manifolds are dominated by the bis(diphenylamino) → bipyridine $\pi\pi$* transition (LLCT). The results support the conclusion drawn from the photophysical properties in that the diphenylamino substituent with strong electron donating properties raises the π HOMO level and hence greatly reduces the metal d_π contribution in **3**. Accordingly, there is an intrinsic difference in the T_1 state between **2** and **3**, in which **2** possesses a large percentage (35.4%) of MLCT, such that its $T_1 \rightarrow S_0$ phosphorescence radiative

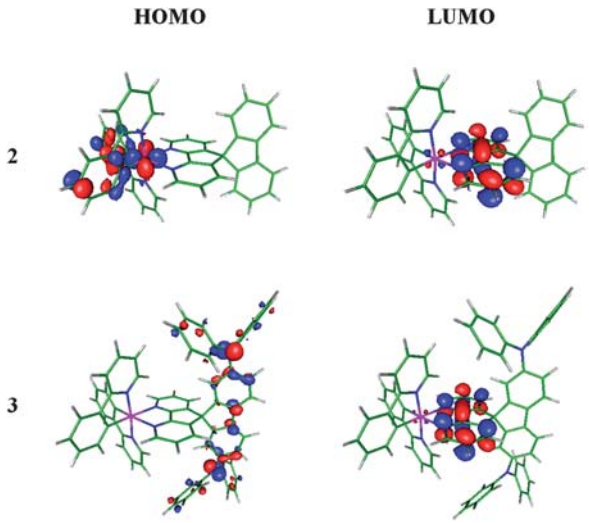

Fig. 4 HOMO and LUMO of complexes **2** and **3**.

lifetime is expected to be short, consistent with the value of of 1.2 μs deduced experimentally. Conversely, due to the dominant ππ* transition with the lack of direct metal d_π involvement, a much longer radiative lifetime is expected for the $T_1 \rightarrow S_0$ radiative decay time, which is deduced to be ~2 millisecond experimentally so that its decay is dominated by the radiationless transition in solution.

Regarding the dominant emission quenching for **3**, a top candidate should be commonly ascribed to the $d_\pi d_{\sigma^*}$ transition involving the bond weakness due to its repulsive anti-bonding character. Therefore, its potential energy surface (PES) is rather shallow (or even repulsive) and may intercept with the ground-state PES, inducing the radiationless deactivation. We then made one step further to analyze the relative energy between the lowest lying transition and the ^{3}MC *dd* state. As a result, the ^{3}MC *dd* state is estimated to be ~50 kcal mol^{-1} higher than that of the lowest lying ππ* state and is thus not likely to serve as the main deactivation channel. Alternatively, due to the rather long radiative lifetime, it is more plausible that the excited-state deactivation in **3** may be simply governed by the mechanism of vibrational matching between T_1 and S_0, known as the energy gap law.[17] As for the polyaromatic molecules, the rate of $S_1 \rightarrow S_0$ internal conversion (IC) due to the vibrational matching could be empirically expresssed as $k_{IC} \sim 10^{13}e^{-\alpha\Delta E}$ where α is a proportionality constant and is taken to be ~0.18, ΔE is the S_1–S_0 energy gap in terms of kcal mol^{-1}.[18] Although an empirical approach for the rate of forbidden T_1–S_0 deactivation (*i.e.* intersystem crossing) is lacking, based on a similar approach of energy gap law, its rate constant based on vibrational matching may be estimated by taking

$$k_{isc} \sim (F)10^{13}e^{-\alpha\Delta E} \quad (1)$$

where we define F to be a forbidden factor, namely $F = k_r$(phosphorescence)/k_r(fluorescence). Though not being directly accessible, k_r(fluorescence) can be estimated according to

$$k_r = 3 \times 10^{-9} n^2 \bar{\nu}_0^2 \int \varepsilon d\bar{\nu} \quad (2)$$

where n is the refractive index of the solvent (~1.341 for CH_3CN at 298 K), $\bar{\nu}_0$ is the energy (in cm^{-1}) corresponding to the peak of the S_0–S_1 absorption,[19] which is taken to be *e.g.* 450 nm for **3**. As a result, k_r is estimated to be 1.2×10^6 s^{-1} and $F = k_r$(phosphorescence)/$1.2 \times 10^6 = 3.62 \times 10^{-4}$ for **3**. On the other hand, for 600 nm emission ($\Delta E \sim 47$ kcal mol^{-1}) the second term in eqn (1), *i.e.* $10^{13}e^{-\alpha\Delta E}$, is then calculated to be $\sim 2.11 \times 10^9$ s^{-1}. Accordingly, $k_{isc} \sim (F)10^{13}e^{-\alpha\Delta E} = 7.64 \times 10^5$ s^{-1}. Taking 4.35×10^2 s^{-1} ($\tau_r = 2.3$ ms for **3**) for the radiative decay rate constant, the emission quantum yield is thus estimated to be as low as 5.7×10^{-4}. Note that due to the property of charge transfer transition for **3** (see Fig. 4), the emission gap is expected to be significantly smaller than 47 kcal mol^{-1} in CH_3CN and thus the quantum yield could be $\ll 5.7 \times 10^{-4}$, rationalizing the unresolvable emission for **3** in CH_3CN (*vide supra*).

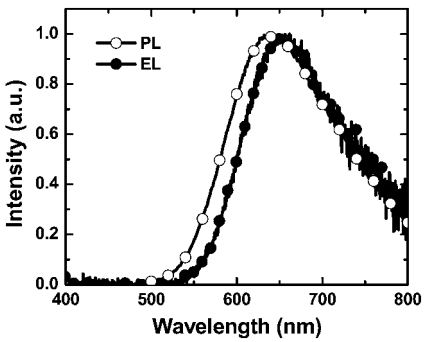

Fig. 5 The neat-film PL spectrum of **3** and the EL spectrum of the LEC based on **3**.

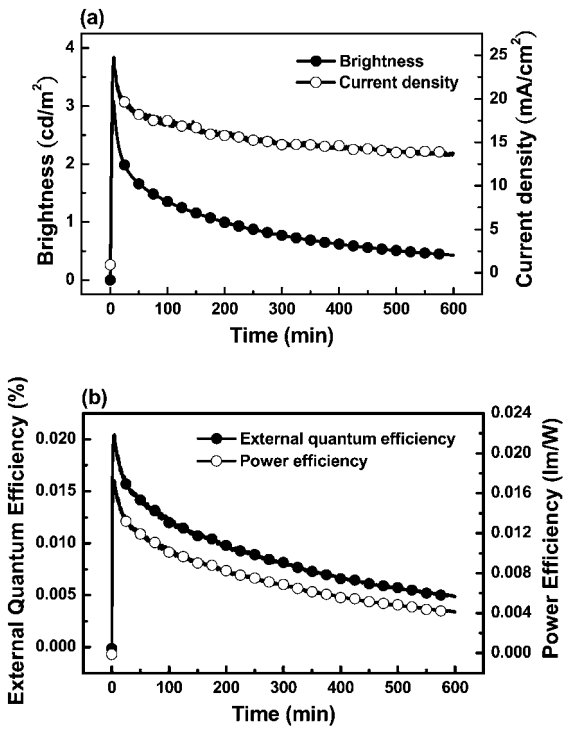

Fig. 6 The time-dependent (a) brightness and current density, and (b) EQE and power efficiency of the LEC device based on **3** with 19 wt.% $BMIM^+(PF_6^-)$.

Fig. 5 depicts the neat-film PL spectrum of **3** and the EL spectrum of the LEC based on **3**. EL spectra are basically similar to PL spectra, indicating similar emission mechanisms. Fig. 6(a) shows the time-dependent brightness and current density under constant biases of 2.4 V for the LEC based on **3** with 19 wt.% $BMIM^+(PF_6^-)$. $BMIM^+(PF_6^-)$ was added to enhance the ionic conductivity of the emissive layer and thus to accelerate the device response. After the bias was applied, the device current first rapidly increased and then reached a maximum, followed by a relatively slow decrease. The brightness followed the same time-dependent trend of the device current and reached a maximum brightness of 3 cd m^{-2} at 2.4 V. Corresponding time-dependent external quantum efficiencies (EQEs) and power efficiencies of the same device are shown in Fig. 6(b). When a forward bias was just applied, the EQE was rather low due to poor carrier injection. During the formation of the p- and n-type regions near electrodes, the capability of carrier injection was improved and the EQE thus rose rapidly. The peak EQE, peak current efficiency and peak power efficiency at 2.4 V are 0.020%, 0.013 cd A^{-1} and 0.017 lm/W, respectively. The drop of efficiency and brightness after reaching the peak value may be associated with a number of factors. Before the current reaches a steady value, the carrier recombination zone may keep moving closer to one electrode due to the discrepancy in electron and hole mobilities, which would induce exciton quenching. Further, the decrease in brightness/efficiency under a constant bias was irreversible and may thus be rationally associated with the degradation of the emissive material during the LEC operation.[20] The low device efficiencies are in accordance with the low PL quantum yield, arising from the ligand-centered radiationless deactivation (*vide supra*).

Conclusion

To sum up, we report here a strategic design and synthesis of a bis(diphenylamino)-9,9′-spirobifluorene functionalized Ir(III) complex, complex **3**. As a result, both electron and hole transporting sites are located at the designated moieties, *i.e.* 4,5-diazafluorene and bis(diphenylamino) sites, respectively, while the whole Ir(III) complex serves as a luminescence unit, achieving a conceptual design of a three-in-one (luminescence chromophore and electron and hole transport) system suited for OLEDs. Unfortunately, owing to the far lifting of the π-electron from -NPh_2, there is virtually no ^{3}MLCT contribution to the lowest transition for **3** in the triplet manifold. On the other hand, the energy gap law may play a role in governing the deactivation process in **3**. The LEC device based on **3** shows characteristic LEC behavior. However, the current device suffers low device efficiency, the results of which are in accordance with the observation of low PL quantum yield that is verified by theoretical calculation. Future strategic design for an ideal three-in-one system may lie in optimizing the ratio for metal d_π *versus* ligand π contribution to enhance the radiative decay rate. Alternatively, another feasible approach is to replace Ir(III) by other late transition metals, *e.g.* Os(II) ion, such that the d_π energy could be raised due to its lower oxidation potential.[21] We thus believe that the conceptual design presented here and its corresponding photophysics and rationalization should provide valuable information for future progress *en route* to an ideal three-in-one system suited for OLEDs.

Acknowledgements

This work was supported by the National Science Council and Ministry of Economic Affairs of Taiwan. We are also grateful to the National Center for High-Performance Computing for computer time and facilities.

References

1 (*a*) M. A. Baldo, D. F. O'Brien, Y. You, A. Shoustikov, S. Sibley, M. E. Thompson and S. R. Forrest, *Nature*, 1998, **395**, 151; (*b*) S. Welter, K. Brunner, J. W. Hofstraat and L. De Cola, *Nature*, 2003, **421**, 54; (*c*) H. Yersin, *Top. Curr. Chem.*, 2004, **241**, 1; (*d*) E. Holder, B. M. W. Langeveld and U. S. Schubert, *Adv. Mater.*, 2005, **17**, 1109; (*e*) R. C. Evans, P. Douglas and C. J. Winscom, *Coord. Chem. Rev.*, 2006, **250**, 2093; (*f*) W.-Y. Wong and C.-L. Ho, *Coord. Chem. Rev.*, 2009, **253**, 1709; (*g*) W.-Y. Wong and C.-L. Ho, *J. Mater. Chem.*, 2009, **19**, 4457.
2 T. Fuhrmann and J. Salbeck, *MRS Bull.*, 2003, **28**, 354.
3 (*a*) C.-H. Yang, Y.-M. Cheng, Y. Chi, C.-J. Hsu, F.-C. Fang, K.-T. Wong, P.-T. Chou, C.-H. Chang, M.-H. Tsai and C.-C. Wu, *Angew. Chem., Int. Ed.*, 2007, **46**, 2418; (*b*) G. Zhou, W.-Y. Wong, B. Yao, Z. Xie and L. Wang, *Angew. Chem., Int. Ed.*, 2007, **46**, 1149; (*c*) S.-J. Liu, Q. Zhao, Y. Deng, Y.-J. Xia, J. Lin, Q.-L. Fan, L.-H. Wang and W. Huang, *J. Phys. Chem. C*, 2007, **111**, 1166; (*d*) W.-Y. Wong, G.-J. Zhou, X.-M. Yu, H.-S. Kwok and B.-Z. Tang, *Adv. Funct. Mater.*, 2006, **16**, 838; (*e*) C. Rothe, S. King and A. Monkman, *Nat. Mater.*, 2006, **5**, 463; (*f*) M. S. Lowry and S. Bernhard, *Chem.–Eur. J.*, 2006, **12**, 7970; (*g*) S. M. King, H. A. Al-Attar, R. J. Evans, A. Congreve, A. Beeby and A. P. Monkman, *Adv. Funct. Mater.*, 2006, **16**, 1043; (*h*) T.-H. Kim, H. K. Lee, O. O. Park, B. D. Chin, S.-H. Lee and J. K. Kim, *Adv. Funct. Mater.*, 2006, **16**, 611; (*i*) E. A. Plummer, A. Van Dijken, H. W. Hofstraat, L. De Cola and K. Brunner, *Adv. Funct. Mater.*, 2005, **15**, 281; (*j*) C.-M. Che, S.-C. Chan, H.-F. Xiang, M. C. W. Chan, Y. Liu and Y. Wang, *Chem. Commun.*, 2004, 1484; (*k*) C.-H. Tao, N. Zhu and V. W.-W. Yam, *Chem.–Eur. J.*, 2005, **11**, 1647; (*l*) J. Kavitha, S.-Y. Chang, Y. Chi, J.-K. Yu, Y.-H. Hu, P.-T. Chou, S.-M. Peng, G.-H. Lee, Y.-T. Tao, C.-H. Chien and A. J. Carty, *Adv. Funct. Mater.*, 2005, **15**, 223; (*m*) S.-Y. Chang, J. Kavitha, S.-W. Li, C.-S. Hsu, Y. Chi, Y.-S. Yeh, P.-T. Chou, G.-H. Lee, A. J. Carty, Y.-T. Tao and C.-H. Chien, *Inorg. Chem.*, 2006, **45**, 137; (*n*) Z. He, W.-Y. Wong, X. Yu, H.-S. Kwok and Z. Lin, *Inorg. Chem.*, 2006, **45**, 10922; (*o*) B. Ma, P. I. Djurovich, S. Garon, B. Alleyne and M. E. Thompson, *Adv. Funct. Mater.*, 2006, **16**, 2438; (*p*) F. N. Castellano, I. E. Pomestchenko, E. Shikhova, F. Hua, M. L. Muro and N. Rajapakse, *Coord. Chem. Rev.*, 2006, **250**, 1819; (*q*) M. Cocchi, D. Virgili, V. Fattori, D. L. Rochester and J. A. G. Williams, *Adv. Funct. Mater.*, 2007, **17**, 285; (*r*) Y. Y. Scaffidi-Domianello, A. A. Nazarov, M. Haukka, M. Galanski, B. K. Keppler, J. Schneider, P. Du, R. Eisenberg and V. Y. Kukushkin, *Inorg. Chem.*, 2007, **46**, 4469.
4 (*a*) C. Adachi, M. A. Baldo, M. E. Thompson and S. R. Forrest, *J. Appl. Phys.*, 2001, **90**, 5048; (*b*) Y. Kawamura, K. Goushi, J. Brooks, J. J. Brown, H. Sasabe and C. Adachi, *Appl. Phys. Lett.*, 2005, **86**, 071104; (*c*) E. L. Williams, K. Haavisto, J. Li and G. E. Jabbour, *Adv. Mater.*, 2007, **19**, 197.
5 (*a*) K.-T. Wong, Y.-Y. Chien, R.-T. Chen, C.-F. Wang, Y.-T. Lin, H.-H. Chiang, P.-Y. Hsieh, C.-C. Wu, C. H. Chou, Y. O. Su, G.-H. Lee and S.-M. Peng, *J. Am. Chem. Soc.*, 2002, **124**, 11576; (*b*) C.-C. Wu, T.-L. Liu, W.-Y. Hung, Y.-T. Lin, K.-T. Wong, R.-T. Chen, Y.-M. Chen and Y. –Y. Chien, *J. Am. Chem. Soc.*, 2003, **125**, 3710; (*c*) K.-T. Wong, R.-T. Chen, F.-C. Fang, C.-C. Wu and Y.-T. Lin, *Org. Lett.*, 2005, **7**, 1979.
6 K.-T. Wong, H.-F. Chen and F.-C. Fang, *Org. Lett.*, 2006, **8**, 3501.
7 H.-C. Su, F.-C. Fang, T.-Y. Hwu, H.-H. Hsieh, H.-F. Chen, G.-H. Lee, S.-M. Peng, K.-T. Wong and C.-C. Wu, *Adv. Funct. Mater.*, 2007, **17**, 1019.
8 Z. Otwinowski and W. Minor, In *Methods in Enzymology: Macromolecular Crystallography, Part A*; C. W. Carter Jr.; R. M. Sweet Eds; Academic Press: San Diego, vol. 276, 2005.
9 G. M. Sheldrick, *SHELXL-97, Program for the Solution of Crystal Structures*, University of Göttingen, Göttingen, Germany, 1997.

10 (*a*) C. Lee, W. Yang and R. G. Parr, *Phys. Rev. B*, 1988, **37**, 785; (*b*) A. D. Becke, *J. Chem. Phys.*, 1993, **98**, 5648.
11 (*a*) P. J. Hay and W. R. Wadt, *J. Chem. Phys.*, 1985, **82**, 270; (*b*) W. R. Wadt and P. J. Hay, *J. Chem. Phys.*, 1985, **82**, 284; (*c*) P. J. Hay and W. R. Wadt, *J. Chem. Phys.*, 1985, **82**, 299.
12 P. C. Hariharan and J. A. Pople, *Mol. Phys.*, 1974, **27**, 209.
13 (*a*) C. Jamorski, M. E. Casida and D. R. Salahub, *J. Chem. Phys.*, 1996, **104**, 5134; (*b*) M. Petersilka, U. J. Grossmann and E. K. U. Gross, *Phys. Rev. Lett.*, 1996, **76**, 1212; (*c*) R. Bauernschmitt, R. Ahlrichs, F. H. Hennrich and M. M. Kappes, *J. Am. Chem. Soc.*, 1998, **120**, 5052; (*d*) M. E. Casida, *J. Chem. Phys.*, 1998, **108**, 4439; (*e*) R. E. Stratmann, G. E. Scuseria and M. J. Frisch, *J. Chem. Phys.*, 1998, **109**, 8218.
14 *Gaussian 03, revision C.02* Gaussian, Inc., Wallingford CT, 2004.
15 (*a*) S. I. Gorelsky, *AOMix: Program for Molecular Orbital Analysis,*http://www.sg-chem.net/, University of Ottawa, 2007; (*b*) S. I. Gorelsky and A. B. P. Lever, *J. Organomet. Chem.*, 2001, **635**, 187.
16 S. T. Parker, J. D. Slinker, M. S. Lowry, M. P. Cox, S. Bernhard and G. G. Malliaras, *Chem. Mater.*, 2005, **17**, 3187.
17 (*a*) E. M. Kober, J. V. Caspar, R. S. Lumpkin and T. J. Meyer, *J. Phys. Chem.*, 1986, **90**, 3722; (*b*) J. A. Treadway, B. Loeb, R. Lopez, P. A. Anderson, F. R. Keene and T. J. Meyer, *Inorg. Chem.*, 1996, **35**, 2242.
18 N. J. Turro, *Modern Molecular Photochemistry*, University Science Books, 1991, Chapter 6.
19 S. J. Strickler and R. A. Berg, *J. Chem. Phys.*, 1962, **37**, 814.
20 G. Kalyuzhny, M. Buda, J. McNeill, P. Barbara and A. J. Bard, *J. Am. Chem. Soc.*, 2003, **125**, 6272.
21 Y. Chi and P.-T. Chou, *Chem. Soc. Rev.*, 2007, **36**, 1421.

